425
11-3-80
26. 1987

DOE/JPL/954331-80/11

SILICON MATERIALS TASK OF THE LOW-COST SOLAR ARRAY PROJECT (PHASE IV)

MASTER

Effects of Impurities and Processing on Silicon Solar Cells

Nineteenth Quarterly Report for April—June 1980

By
R. H. Hopkins
J. R. Davis
A. Rohatgi
R. B. Campbell
P. Rai-Choudhury
M. H. Hanes
H. C. Mollenkopf
J. R. McCormick

July 1980

Work Performed Under Contract No. NAS-7-100-954331

Westinghouse Research & Development Center
Pittsburgh, Pennsylvania

and

Hemlock Semiconductor Corporation
Michigan

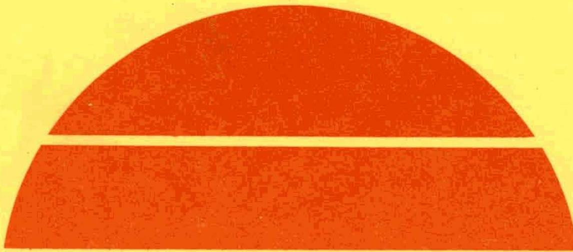

U.S. Department of Energy

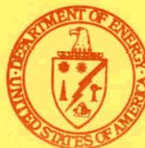

Solar Energy

DISTRIBUTION OF THIS DOCUMENT IS UNLIMITED

DISCLAIMER

This report was prepared as an account of work sponsored by an agency of the United States Government. Neither the United States Government nor any agency Thereof, nor any of their employees, makes any warranty, express or implied, or assumes any legal liability or responsibility for the accuracy, completeness, or usefulness of any information, apparatus, product, or process disclosed, or represents that its use would not infringe privately owned rights. Reference herein to any specific commercial product, process, or service by trade name, trademark, manufacturer, or otherwise does not necessarily constitute or imply its endorsement, recommendation, or favoring by the United States Government or any agency thereof. The views and opinions of authors expressed herein do not necessarily state or reflect those of the United States Government or any agency thereof.

DISCLAIMER

Portions of this document may be illegible in electronic image products. Images are produced from the best available original document.

DISCLAIMER

"This book was prepared as an account of work sponsored by an agency of the United States Government. Neither the United States Government nor any agency thereof, nor any of their employees, makes any warranty, express or implied, or assumes any legal liability or responsibility for the accuracy, completeness, or usefulness of any information, apparatus, product, or process disclosed, or represents that its use would not infringe privately owned rights. Reference herein to any specific commercial product, process, or service by trade name, trademark, manufacturer, or otherwise, does not necessarily constitute or imply its endorsement, recommendation, or favoring by the United States Government or any agency thereof. The views and opinions of authors expressed herein do not necessarily state or reflect those of the United States Government or any agency thereof."

This report has been reproduced directly from the best available copy.

Available from the National Technical Information Service, U. S. Department of Commerce, Springfield, Virginia 22161.

Price: Paper Copy $6.00
Microfiche $3.50

DOE/JPL/954331-80/11
Distribution Category UC-63b

SILICON MATERIALS TASK OF THE LOW-COST SOLAR ARRAY PROJECT (PHASE IV)

Effects of Impurities and Processing on Silicon Solar Cells

Nineteenth Quarterly Report

July 1980

April 1980-June 1980

R. H. Hopkins, J. R. Davis, A. Rohatgi
R. B. Campbell, and P. Rai-Choudhury, and M. H. Hanes
Westinghouse Research and Development Center
and
H. C. Mollenkopf and J. R. McCormick
Hemlock Semiconductor Corporation

Contract No. 954331

The JPL Low-Cost Silicon Solar Array Project is sponsored by the U. S. Department of Energy and forms part of the Solar Photovoltaic Conversion Program to initiate a major effort toward the development of low-cost solar arrays. This work was performed for the Jet Propulsion Laboratory, California Institute of Technology by agreement between NASA and DOE.

Westinghouse R&D Center
1310 Beulah Road
Pittsburgh, Pennsylvania 15235

DISTRIBUTION OF THIS DOCUMENT IS UNLIMITED

TABLE OF CONTENTS

		Page
1.	SUMMARY	1
2.	INTRODUCTION	3
3.	TECHNICAL PROGRESS	4
	3.1 Crystal Growth and Analysis	4
	3.1.1 Ingot Preparation	4
	3.1.2 Ingot Evaluation	4
	3.2 Deep Level Measurements	15
	3.3 Polycrystalline Material and Cell Evaluation	15
	3.4 Permanence of Impurity Effects in Silicon and Silicon Solar Cells	24
	3.4.1 Accelerated Aging	24
	3.4.2 Thermally Activated Diffusion	24
	3.4.3 Combined Thermal and Electrical Stress	25
	3.5 Thermochemical Processing	26
	3.6 Impurity Effects in High Efficiency Cells	26
4.	CONCLUSIONS	31
5.	PROGRAM STATUS	33
	5.1 Present Status	33
	5.2 Future Activity	33
6.	REFERENCES	34
7.	ACKNOWLEDGEMENTS	35

LIST OF TABLES

Table		Page
1	Ingot Impurity, Structure, and Task	8
2	Ingot Impurity Concentration.	9
3	Best Estimate of Impurity Concentrations.	11
4	Ingot Electrical and Defect Characteristics	12
5	Ingot Carbon and Oxygen Concentrations.	14
6	DLTS Results on Single Crystals	16
7	Expected and Observed Cell Performance From Ingots 206 to 211	17
8	DLTS Results for Ingot 202-Ti-Poly.	20
9	DLTS Results for Ingot 203-V-Poly	21
10	Cell Data for Impurity Doped Polycrystalline Ingots	22

LIST OF FIGURES

Figure		Page
1	Microstructure of Ingot W214-V-006 Poly. Optical micrograph, 6X.	6
2	Microstructure of Ingot W215-Mo-009 Poly. Optical micrograph, 6X.	7
3	Microstructure of wafers cut from ingot W203V005-S Optical micrograph, 6X. The photograph is also very typical of the features observed in Ingot W202Ti013.	19

TECHNICAL CONTENT STATEMENT

This report was prepared as an account of work sponsored by the United States Government. Neither the United States nor the United States Department of Energy, nor any of their employees, nor any of their contractors, sub-contractors, or their employees, makes any warranties, express or implied, or assumes any legal liability or responsibility for the accuracy, completeness or usefulness of any information, apparatus, product or process disclosed, or represents that its use would not infringe privately owned rights.

NEW TECHNOLOGY

No new technology is reportable for the period covered by this report.

I. SUMMARY

The overall objective of this program is to define the effects of impurities, various thermochemical processes, and any impurity-process interactions upon the performance of terrestrial solar cells. The results of the study form a basis for silicon producers, wafer manufacturers, and cell fabricators to develop appropriate cost-benefit relationships for the use of less pure, less costly solar grade silicon.

Nine 4 ohm-cm p type silicon ingots were grown and evaluated in support of the experimental program this quarter. Of these, three were polycrystalline ingots doped with Cr, Mo, and V, respectively, produced under conditions which successfuly eliminated the metal-rich inclusions formed when growth of these heavily-doped specimens was attempted during the last quarter.

Evaluation of polycrystalline ingots doped to the mid 10^{13} cm^{-3} range with Ti or V showed little evidence for grain boundary segregation. Deep level spectroscopy on both as-grown wafers and solar cells showed little variation in impurity concentration from place to place across the ingot regardless of the presence of grain boundaries or other structural features. Solar cell behavior could be correlated with the electrically active impurity concentration.

Deep level spectroscopy was also used to monitor the electrically active impurity concentrations in ingots to be used for process studies, aging experiments, and high efficiency cells. In each case, the observed solar cell performance correlated very well with the performance projected on the basis of the measured impurity concentration.

The basic aspects of a model to describe efficiency behavior in high efficiency cells have been formulated and a computer routine is being implemented for back field type devices to analyze the functional

relationships between impurity concentrations and cell performance. Qualitatively, the model projects that the threshold for impurity-induced performance loss will be lower in high efficiency devices than in comparable standard devices.

2. INTRODUCTION

This is the nineteenth quarterly report describing activities conducted under JPL Contract 954331, and is the second report of the Phase IV studies.

In Phase III, "An Investigation of the Effects of Impurities and Processing on Silicon Solar Cells," effects of thermal processes, impurities, and impurity-process interactions were determined and documented. The development of this data base has led to a more precise definition of what constitutes an acceptable "Solar Grade" Silicon. In addition, it has provided silicon manufacturers with a rationale for selection of construction materials; moreover, it has helped ingot, sheet, or ribbon manufacturers to specify the purity of silicon feedstocks. Finally, it has enabled cell manufacturers to define acceptable wafer purities for cell fabrication and to choose processes which minimize adverse impurity effects. In short, the impurity effect data provide a basis for cost-benefit analysis to producers and users of Solar Grade Silicon.

In Phase IV of this program, the approaches and techniques developed in Phase III are being extended to several new areas, as well as to developing an improved data base for aging effects and certain process-related phenomena. The Phase IV tasks include (1) evaluation, by previously developed process techniques, of the properties of silicon produced by experimental low cost processes; (2) extending threshold impurity concentration data to high efficiency cells; (3) measuring the effects of interaction between impurities and grain boundaries in polycrystalline solar cells; (4) evaluating the long term effects of impurities in solar cells; and (5) examining the effects of processes such as ion implantation on contaminated solar cells.

3. TECHNICAL PROGRESS

3.1 Crystal Growth and Analysis

3.1.1 Ingot Preparation

The second quarter's effort consisted of monocrystalline silicon ingot growth and regrowth of polycrystalline ingots prepared earlier. The polycrystalline ingot regrowth was necessary to replace poly ingots grown in the previous quarter that exhibited metal-rich inclusions when high melt doping levels were employed.

Nine 4 ohm-cm p-type silicon ingots were grown this quarter with each ingot's intentionally added impurity dopant, associated crystalline structure, and task indicated in Table 1. In accordance with the earlier phases of the program, each ingot was prepared by the Czochralski crystal growth method. Details of the crystal growth equipment and conditions can be found in earlier reports[1,2].

3.1.2 Ingot Evaluation

This quarter's ingot growth was initiated with W-213 Pb. As with earlier reports, detailed ingot impurity data are indicated in Table 2, with the listing of ingot identification, intentionally-added target impurity concentration, ingot impurity concentration based on melt analysis by atomic absorption (calculated concentration), and ingot seed impurity concentration measured by spark source mass spectrometry[2,3].

Two W-213 Pb-doped ingots were attempted, each melt containing greater than 1% by weight intentionally added 99.999% pure Pb dopant. Both ingots had no detectable Pb Table 2, (W-213Pb) as indicated by atomic absorption-calculated concentration, and spark source mass spectrometer analysis. The inability to detect Pb was consistent with the visible Pb vaporization cloud observed during crystal growth (Pb vaporization pressure greater than 1 mm Hg at 1400°C).

Polycrystalline ingots W-214 V, W-215 Mo and W-216 Cr were grown at reduced dopant concentrations to replace poly ingots W-200 V, W-201 Mo, and W-204 Cr grown during the previous quarter. This eliminated the metal-rich inclusions formed in the earlier poly growths as well as the submillimeter-size grain structure. Figures 1 and 2 illustrate the 1 to 3 millimeter sized grains typical of ingots W-214 to W-216. The absence of inclusions is clear from the microstructures shown and is also supported by the good agreement between the spark source mass spectroscopy data and calculated ingot concentrations, Table 2. In comparison the mass spectrographic data for ingots W-200, W-201 and W-204 showed large and variable values of impurity content due to inclusions.

As expected, the calculated impurity concentration data obtained from atomic absorption analysis of the melt after ingot growth continues to agree quite satisfactorily with the target values.

A best estimate[3] of the impurity concentrations for Phase IV ingots is listed in Table 3. The spark source data for the poly ingots W-200, W-201, and W-204 were omitted from the list due to the analytical problems cited above. The best estimate for W-212 was obtained from the calculated value. Additional spark source evaluations on W-212 will be completed early the next quarter to determine the reason for the difference between the calculated and spark source results.

The resistivity and etch pit data for all of Phase IV ingots are indicated in Table 4. The values for each ingot continue to fall close to the norms established in earlier phases[3] of this program. Etch pit analysis is not applicable to the polycrystalline samples.

The carbon and oxygen concentrations of each odd-numbered ingot were measured by infrared absorption at room temperature using Fourier Transform Infrared Spectroscopy. The amplitude of the absorption peaks at 606 cm^{-1} and 1107 cm^{-1} is proportional to the carbon and oxygen concentrations, respectively. The constants of proportionality used in these measurements were 2.2 for carbon and 9.6 for oxygen[2]. Normal carbon and oxygen concentrations found in Cozhcralski grown material are

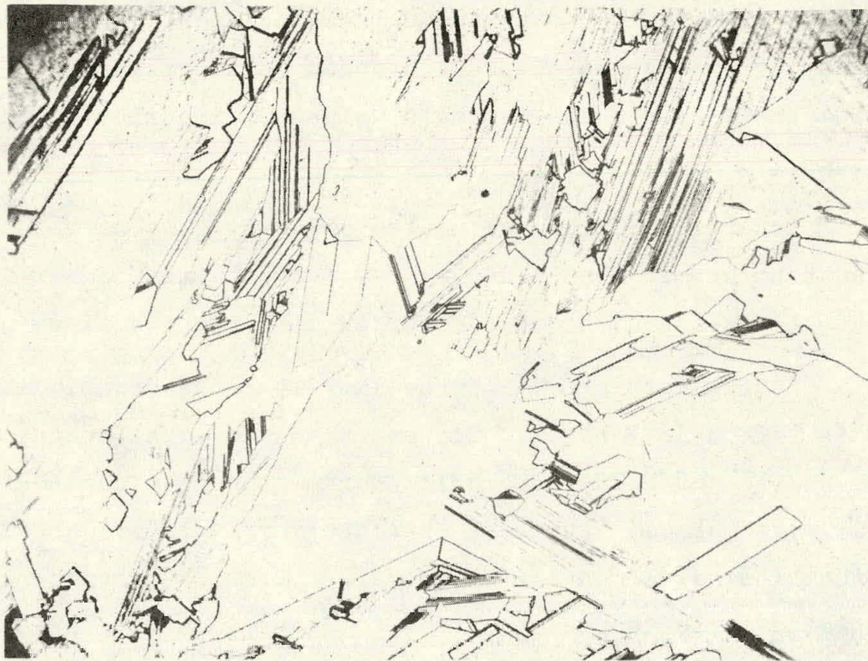

Figure 1 Microstructure of Ingot W214-V-006 Poly. Optical micrograph, 6X.

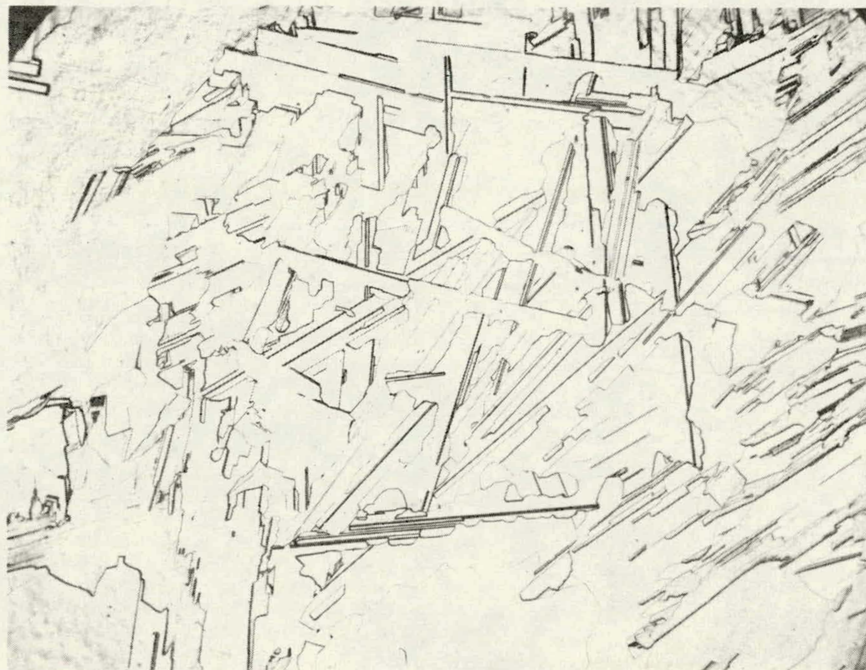

Figure 2 Microstructure of Ingot W215-Mo-009 Poly. Optical micrograph, 6X.

TABLE 1. INGOT IMPURITY, STRUCTURE, AND TASK

Impurity	Structure	Task
Pb	Single	Processing
V	Poly	Poly
Mo	Poly	Poly
Cr	Poly	Poly
Ta	Single	Processing
Ta	Single	Processing
V	Single	High Efficiency
W	Single	Processing
Ni	Single	Permanence

TABLE 2. INGOT IMPURITY CONCENTRATION

Ingot Identification	Target Concentration ($x10^{15}$ atoms/cm^3)	Calculated Concentration ($x10^{15}$ atoms/cm^3)	Mass Spec. Analysis ($x10^{15}$ atoms/cm^3)
W-198-00-000	None	N/A	None
W-199-00-000	None	N/A	None
W-200-V-004-Poly	0.4	0.38	18.5*
W-201-Mo-007-Poly	0.005	0.003	77*
W-202-Ti-013-Poly	0.02	0.018	<0.25
W-203-V-005-Poly	0.04	0.053	<0.15
W-204-Cr-008-Poly	1.0	0.82	1322*
W-205-Fe-009-Poly	0.8	Processing	Processing
W-206-V-006	0.02	0.026	<0.15
W-207-Mo-008	0.002	0.002	<0.5
W-208-Cr-009	0.2	0.19	0.6
W-209-Ti-014	0.02	0.024	<0.25
W-210-Ti-015	0.08	0.10	<0.25
W-211-Cu-007	1.0	1.0	2.6
W-212-Cu-008	10	12.5	80.5
W-213-Pb-001	Max. Conc.	Non Detectable	<0.10+
W-214-V-007-Poly	0.20	0.30	0.55**
W-215-Mo-009-Poly	0.0025	0.002	<0.5**
W-216-Cr-010-Poly	0.80	0.64	2.2**
W-217-Ta-005	0.00015	0.0003	<0.5
W-218-Ta-006	0.000065	0.0001	<0.5
W-219-V-008	0.007	Processing	Processing

TABLE 2. INGOT IMPURITY CONCENTRATION (continued)

Ingot Identification	Target Concentration ($x10^{15}$ atoms/cm^3)	Calculated Concentration ($x10^{15}$ atoms/cm^3)	Mass Spec. Analysis ($x10^{15}$ atoms/cm^3)
W-220-W-005	0.0008	Processing	Processing
W-221-Ni-005	10	Processing	Processing

* Ingots contain metal-rich inclusions due to constitutional supercooling.
** Ingots regrown to remove metal-rich inclusions due to constitutional supercooling.
\+ Pb dopant vaporized on two separate ingot growths.

TABLE 3. BEST ESTIMATE OF IMPURITY CONCENTRATIONS

Ingot Identification	Best Estimate of Impurity Conc. ($\times 10^{15}$ atoms/cm^3)
W-198-00-000	NA
W-199-00-000	NA
W-200-V-004-Poly	0.38
W-201-Mo-007-Poly	0.003
W-202-Ti-013-Poly	0.018
W-203-V-005-Poly	0.05
W-204-Cr-008-Poly	0.82
W-205-Fe-009-Poly	Processing
W-206-V-006	0.026
W-207-Mo-008	0.002
W-208-Cr-009	0.19
W-209-Ti-014	0.02
W-210-Ti-015	0.10
W-211-Cu-007	1.8
W-212-Cu-008	12.5
W-213-Pb-001	ND+
W-214-V-007-Poly	0.4
W-215-Mo-009-Poly	0.002
W-216-Cr-010-Poly	1.0
W-217-Ta-005	0.0003
W-218-Ta-006	0.0001
W-219-V-008	Processing
W-220-W-005	Processing
W-221-Ni-005	Processing

+ ND - Non Detectable

TABLE 4. INGOT ELECTRICAL AND DEFECT CHARACTERISTICS

Ingot Identification	TGT Resistivity (ohm-cm)	Actual Resistivity (ohm-cm)	Etch Pit Density ($/cm^2$)
W-198-00-000	4.0	4.1-3.9	0-3K
W-199-00-000	4.0	3.7-3.5	1-5K
W-200-V-004/Poly	4.0	3.6-2.3	NA
W-201-Mo-007/Poly	4.0	3.8-2.3	NA
W-202-Ti-013/Poly	4.0	5.3-3.9	NA
W-203-V-005/Poly	4.0	4.4-3.8	NA
W-204-Cr-008/Poly	4.0	4.7-4.3	NA
W-205-Fe-009/Poly	4.0	Incomplete	Incomplete
W-206-V-006	4.0	3.7-3.6	0-5K
W-207-Mo-008	4.0	3.8-3.5	0-15K
W-208-Cr-009	4.0	3.7-3.5	0-15K
W-209-Ti-014	4.0	4.0-3.3	0-10K
W-210-Ti-015	4.0	4.0-3.5	0-5K
W-211-Cu-007	4.0	4.0-3.1	0-5K
W-212-Cu-008	4.0	3.9-3.3	5-20K
W-213-Pb-001	4.0	3.3-2.7	10-20K
W-214-V-007-Poly	4.0	3.8-3.1	NA
W-215-Mo-009-Poly	4.0	3.8-1.7	NA
W-216-Cr-010-Poly	4.0	7.6-2.9	NA
W-217-Ta-005	4.0	3.5-3.0	0-10K
W-218-Ta-006	4.0	3.7-3.2	0-5K

TABLE 4. INGOT ELECTRICAL AND DEFECT CHARACTERISTICS

Ingot Identification	TGT Resistivity (ohm-cm)	Actual Resistivity (ohm-cm)	Etch Pit Density ($/cm^2$)
W-219-V-008	4.0	Processing	Processing
W-220-W-005	4.0	Processing	Processing
W-221-Ni-005	4.0	Processing	Proceesing

TABLE 5. INGOT CARBON AND OXYGEN CONCENTRATIONS

Ingot Identification	Carbon Concentration ($\times 10^{16}$ atoms/cm^3)	Oxygen Concentration ($\times 10^{16}$ atoms/cm^3)
W-201-Mo-007/P	7.0	120
W-203-V-005/P	12	116
W-205-Fe-009/P	8.0	66
W-207-Mo-008	5.4	84
W-209-Ti-014	6.4	120
W-211-Cu-007	6.0	111
W-213-Pb-001	8.0	105
W-215-Mo-009-Poly	10.0	110
W-217-Ta-005	12.0	98
W-219-V-008	25.0	84
W-221-Ni-005	Processing	Processing

in the range of 2.5 to $5x10^{17}$ atoms/cm^3 for carbon and 5 to $150x10^{16}$ atoms/cm^3 for oxygen. As usual, no significant deviations from these values were observed this quarter as indicated in Table 5.

3.2 Deep Level Measurements

Deep level transient spectroscopy (DLTS) and solar cell measurements have been performed on ingots 206, 207, 208, 209, 210, and 211 to monitor impurity behavior and response of impurities to cell processing. Thirty mil diameter Schottky barrier diodes were fabricated on the p-type wafers for the DLTS measurements. The solar cell mesas were subdivided into thirty mil diameter diodes to study the response of the impurities to the solar cell diffusion near the junction.[3]

The DLTS results on the as-grown wafers and solar cells are listed in Table 6, along with the activity ratios (ratio of the electrically active impurity concentration to the metallurgical concentration in the wafer) of the impurities. These are the same deep levels, for Mo, Ti, V and Cr impurities we have previously reported[3]. No deep level was found in the Cu-contaminated crystal. Most of the data in Table 6 are consistent with our previous results[3]; i.e., the activity ratios for Mo, Ti, V and Cr are 1, 0.4, 0.28 and 0.23, respectively. Slight variations in these numbers are attributed to the uncertainties in the best estimate metallurgical concentration numbers (about a factor of 2).

Table 7 illustrates a comparison of the expected cell efficiency calculated from the model[3] and the observed cell data. Again, a reasonable agreement was observed in most cases.

3.3 Polycrystalline Material and Cell Evaluation

Solar cells have been fabricated from polycrystalline wafers purposely contaminated with an intermediate concentration of Ti or V (ingots 202-Ti and 203-V). DLTS measurements were then performed to identify any influence of microstructure on the active impurity concentration. A large numer of 30 mil and 16 mil diameter Ti-Au Schottky barrier diodes were made on the wafers for the DLTS measurements,

TABLE 6

DLTS RESULTS ON SINGLE CRYSTALS

Ingot ID	Best Estimate of Metallurgical Impurity Concentration (N_M)	Active Impurity Concentration (cm^{-3})		$\frac{N_{TW}}{N_M}$
		In the Wafer N_{TW}	In the Cell (near junction) N_{TC}	
206-V	2.6×10^{13}	6.43×10^{12}	undetectable	0.25
207-Mo	2.0×10^{13}	2.2×10^{12}	9×10^{11}	1.1
208-Cr	1.9×10^{14}	3.91×10^{13}	undetectable	0.21
209-Ti	2.0×10^{13}	8.12×10^{12}	No data	0.40
210-Ti	1.0×10^{14}	2.91×10^{13}	No data	0.30
211-Cu	1.8×10^{15}	undetectable	No data	-

TABLE 7

EXPECTED AND OBSERVED CELL PERFORMANCE FROM INGOTS 206 to 211

Ingot ID	Target Impurity Concentration cm^{-3}	Expected Cell Performance η/η_B	Observed Cell Performance η/η_B
206-V	2×10^{13}	0.78	0.77
207-Mo	2×10^{12}	0.78	0.81
208-Cr	1.9×10^{14}	0.81	0.94
209-Ti	2×10^{13}	0.68	0.57
210-Ti	1.0×10^{14}	0.50	0.50
211-Cu	1.8×10^{15}	1.0	0.99

and the results are compiled in Tables 8 and 9. Optical micrographs of the ingot wafer showed a variety of structural features including twins and grain boundaries, e.g. Figure 3. Some of the diodes overlay these microstructural boundaries while others encompass almost none of these defects. The polycrystalline cell data along with similar data from single crystal cells containing about the same amount of impurity are shown in Table 10.

The preliminary data in Tables 8 and 9 imply that regardless of the microstructural variation of the silicon under the diodes, there is only a small variation in the active Ti or V concentrations over the area of the wafer. This suggests no appreciable impurity segregation at structural defects in these ingots.

The average active V concentration in wafers from ingot 203-V-Poly was 1.7×10^{13} cm^{-3}. The expected active vanadium concentration in a single crystal wafer containing 5×10^{13} cm^{-3}V would be 1.4×10^{13} cm^{-3} (based on the activity ratio of 0.28). This indicates that, in this concentration range of the V impurity, there is no appreicable influence of microstructural features on the activity of the vanadium. The DLTS observation is consistent with the cell data in Table 10, which show that the performance of cells from ingot 203-V-poly is nearly the same as expected from a single crystal cell with a similar vanadium content. Since in Table 10 the efficiencies are normalized with respect to the single crystal baseline cell efficiency, the somewhat lower normalized efficiency (0.67 instead of 0.70) of the poly cells could be explained by the small adverse effect of the grain boundaries beyond the effect of vanadium itself. It is important to recognize that grain boundaries by themselves can degrade the cell performance. However, if a harmful impurity is present in sufficient quantity then this effect may become secondary ($\frac{1}{\tau} = \frac{1}{\tau_{impurity}} + \frac{1}{\tau_{microstructure}}$).

Figure 3 Microstructure of wafers cut from ingot W203V005-S Optical micrograph, 6X. The photograph is also very typical of the features observed in Ingot W202Ti013.

TABLE 8

DLTS RESULTS FOR INGOT 202-Ti-poly

- Nominal Ti concentration = 1.8×10^{13} cm^{-3}
- Expected active Ti concentration in single crystal = $7.2 \times 10^{12} cm^{-3}$

Schottky barrier diode No.		Concentration of E_V+0.30 eV Trap (cm^{-3})
	Top	1.12×10^{13}
1S	Middle	1.185×10^{13}
	Bottom	1.106×10^{13}
	Top	1×10^{13}
2S	Middle	7.86×10^{12}
	Bottom	1.06×10^{13}
	Top	1.18×10^{13}
3S	Middle	1.03×10^{13}
	Bottom	1.1×10^{13}
	Top	1.23×10^{13}
4S	Middle	1.1×10^{13}
	Bottom	1.14×10^{13}
	Top	1.12×10^{13}
5S	Middle	1.12×10^{13}
	Bottom	1.12×10^{13}

TABLE 9

DLTS RESULTS FOR INGOT 203-V-Poly

- Nominal V concentration = 5.0×10^{13} cm^{-3}
- Expected active V-concentration in single crystal = 1.40×10^{13} cm^{-3}

ID of Schottky barrier diode		Concentration of E_V+0.42eV Trap
2S	Top	1.6×10^{13}
	Bottom	1.6×10^{13}
3S	Top	1.76×10^{13}
	Middle	2.15×10^{13}
	Bottom	1.85×10^{13}
4S	Top	1.57×10^{13}
	Middle	1.6×10^{13}
	Bottom	1.67×10^{13}
1S	Top	1.7×10^{13}
	Middle	1.9×10^{13}
	Bottom	1.9×10^{13}

- Average active concentration $\sim 1.70\times10^{13}$ cm^{-3}

TABLE 10

CELL DATA FOR IMPURITY DOPED POLYCRYSTALLINE INGOTS

Ingot I-D	Impurity Concentration (cm^{-3})	Expected Cell Performance of Single Crystal η/η_B *	Observed Performance of Poly Cell η/η_B *
201-Mo	$3x10^{12}$	0.72	Crystal Breakdown Shorts in the cells
200-V	$3.8x10^{14}$	0.42	"
202-Ti	$1.8x10^{13}$	0.70	0.57 Requires Investigation, suggests segregation
203-V	$5.0x10^{13}$	0.7	0.67 Indicates no significant segregation

* η_B is the single crystal baseline efficiency

The active Ti concentration deduced from the DLTS data on wafers from ingot Ti-202-poly was 1.12×10^{13} cm^{-3}. The expected active Ti concentration in a single crystal wafer containing 1.8×10^{13} cm^{-3} Ti would be 0.72×10^{13} cm^{-3} (based on the activity ratio of 0.40). The normalized efficiency of the poly cell is 0.57, which is much lower than the efficiency of a single crystal cell (0.70) containing 1.8×10^{13} cm^{-3} Ti. These descrepancies could be due to the following: i) an error in the best estimate of the metallurgical Ti concentration, ii) an increase in the activity of Ti due to microstructural defects, or iii) microstructural influence on the cell performance that is larger than the effect of the Ti impurity. The first possibility seems most likely because the observed active Ti concentration is a factor of only 1.4 higher than the active Ti concentration derived from the best estimate of the metallurgical Ti concentration, where an error as high as a factor of 2 is possible. The electrically active Ti concentration of 1.12×10^{13} cm^{-3} in a single crystal represents a metallurgical concentration of 2.8×10^{13} cm^{-3} which in turn gives a normalized single crystal cell performance of 0.63. This is in much better agreement with the observed polycrystalline cell performance of 0.57 and the remaining difference then can be attributed to the influence of grain boundaries.

The second possibility, an increase in Ti activity, is contrary to our previous observation on ingot 102-Ti-poly where there was a slight decrease in the activity of Ti (less than a factor of two). The observed uniformity in active Ti concentration over the wafer is also at variance with the possibility of microstructure-induced increase in the Ti activity.

The third possibility, very large grain boundary effects, seems unlikely because the junction response (leakage current and shunt-resistance) of the cells was quite reasonable. Further work is in progress to check these possibilities.

3.4 Permanence of Impurity Effects in Silicon and Silicon Solar Cells

3.4.1 Accelerated Aging

We reported last quarter[4] the results of accelerated aging behavior for solar cells contaminated with the impurities Ag, Nb, Fe, Mo, Ti and Cr. Among these Cr and Ag- doped solar cells degraded most rapidly as might be expected for a diffusion-controlled thermally activated process. To complete these studies two more ingots doped with Cu and the maximum possible Ag concentration are being subjected to accelerated aging of temperatures between 200 and 800°C. Both of these impurities represent rapidly diffusing species; Ag degrades the cells by reducing bulk lifetime while Cu produces junction degradation thus both mechanisms of cell damage may be evaluated. These experiments now underway will be reported in full when completed.

3.4.2 Thermally Activated Diffusion

The maximum impurity concentration in Czochralski ingots is limited by the effective segregation coefficient of a given impurity and the tendency of the ingot structure to breakdown at high melt impurity concentrations[3]. A second method for introducing impurities in silicon, thermal diffusion, is not limited in this way and we are using this method to (1) introduce higher impurity concentration in solar cells (2) study the thermal activation of the process with respect to aging effects and (3) produce graded impurity concentrations like those in real cells (see comments in section 3.6).

To represent a range of impurity behavior, the elements Fe, Mo, Ti and Cr were selected for the first studies. A 500Å thick layer of each metal was evaporated onto the surface of a precleaned and uncontaminated baseline wafer then diffused into silicon for thirty minutes at a temperature of 800°C. Spreading resistance measurements on the angle lapped wafers will be used to identify suitable temperature-time cycles for each impurity. Later DLTS will be employed to determine the active concentrations for each specimen. These data coupled with solar cell I-V measurements will be used to extend the concentration range over which the aging data extend.

3.4.3 Combined Thermal and Electrical Stress

Because a solar cell operates both at temperatures above ambient and in the presence of an electrical bias a second set of aging experiments will be carried out to identify what effects, if any, the combined stresses produce. Five impurities have been identified for the study and the appropriate impurity concentrations and ingot identifications are listed in Table 11. These are the same impurities examined in the accelerated thermal aging studies.

TABLE 11

INGOTS FOR ACCELERATED AGING WITH ELECTRICAL BIAS

Ingot ID	Best Estimate Impurity Concentration (10^{15} cm^{-3})
W 192 Ag 001	2.2
W 183 Nb 002	<0.009
W 166 Fe 007	1.06
W 167 Nb 001	<0.044
W 056 Cu 005	65
W 123 Ti 008	0.105

A suitable test fixture has been designed and fabricated to bias test up to thirty cells simultaneously. The bias will be $30 ma/cm^2$ on each cell and the first tests will be carried out at 150°C. Solar cells from each of the ingots listed above have already been fabricated and tested to determine the zero time, or baseline, I-V characteristics.

3.5 Thermochemical Processing

Examination of impurity-process interactions is being extended to polycrystalline and ion-implanted silicon. Polycrystalline wafers from ingots W202Ti013, W203V005, W214V007, and W215Mo009 studied for thermochemical gettering effects by subjecting them to $POC\ell_3$ and $HC\ell$-O_2 containing ambients. Temperatures in the range 950 to 1200°C will be employed as described in earlier reports[3]. These impurities represent fast and slow diffusers in silicon. Results of the studies then will be compared to data already obtained with single crystal wafers. So far the initial baseline cell diffusions have been performed.

Wafers from ingots W211Cu007 and W210Ti015 are being used for studies of gettering by Ar ion implantation damage. The effects of this back side gettering, both alone and combined with $POC\ell_3$ and $HC\ell$ gettering will thus be studied for a fast and a slow diffusing impurity. Baseline cell data on each ingot has been obtained and the Ar ion implants will be carried out shortly.

Wafers from ingots W209Ti014, W210Ti015, W211Cu007, and W135Fe005 will be made into solar cells with front junctions formed by the Spire ion implantation process. Comparison of these solar cells with implanted baseline cells and with diffused junction impurity cells will identify any impurity effects which may be ascribed to the ion implantation process itself.

3.6 Impurity Effects in High Efficiency Cells

The substantial cost-benefit of increased solar cell efficiency makes it important to examine the impact of impurities on high efficiency devices. It would be of considerable value if we could project the high efficiency behavior from the existing data base. To this end, the following discussion compares our standard device design with designs capable of higher efficiency.

The standard 4 ohm-cm p-base device is about 275μm thick with an ohmic back surface and 5% contact grid coverage. With no impurities added this device, using AR coating, achieves 14.5% efficiency and has a base diffusion length of 170μm. The efficiency of this conservative design can be improved in several respects. First, the optical efficiency could be increased by the use of a textured surface, multi-layer AR coatings and reduced contact grid coverage. The combined effect of these changes could result in a cell efficiency approaching 15.7%; however, since impurities act primarily to reduce the diffusion length, the improved design would exhibit the same sensitivity to impurities as does the standard device. Therefore this approach is unsuitable for examining the design-dependent impurity effects.

A second method of impurity efficiency is to exploit the voltage/current trade-offs obtained by lowering the base resistivity. In this case, current experience has shown too small an efficiency improvement to be useful for our purpose.

The third and simplest approach is to increase the base-width and use fabrication techniques to maximize the base diffusion length. This has the effect of decoupling the high recombination back surface from the junction and the base region near the junction where the majority of photons are absorbed. The result is increased short-circuit current, open-circuit voltage, and efficiency. Furthermore, this device is accurately described by the same model equations as is the present standard device. While this is clearly not a cost effective means of producing high efficiency cells, it does provide a very simple, easily understood test structure for the impurity effects study.

The final design approach, and the one capable of the highest efficiencies, requires a back surface field along with careful processing, again to maximize base diffusion length. This has the same effects as does the wide base along with the advantage of allowing the use of thin cells. Cells only 50μm thick have been made with efficiencies of 16%. In this case, the impurity model equations apply only approximately,and

a more exact analysis is necessary to determine the detailed relationship between impurity content and cell performance.

We can predict the impurity effect accurately for wide-base devices and approximately for the backfield devices. The impurity model[3] relates the normalized short-circuit current(I_n) to the impurity concentration (N_x) in terms of a threshold concentration (N_{ox}) above which cell performance is substantially degraded

$$\left(\frac{I_{n\infty}}{I_n} - 1\right)^2 = C_1 \left(1 + \frac{N_x}{N_{ox}}\right) \qquad (1)$$

where C_1 0.0121 and $I_{n\infty}$ 1.11 are model constants which we assume will change little for the high efficiency structure. It can be shown that:

$$N_{ox} = \frac{1}{L_{no}^2 \cdot k_x} \qquad (2)$$

where k_x is a constant for impurity x, related to its recombination cross-section which is independent of cell design and L_{no} is the diffusion length in baseline devices (no impurities present).

We can now relate the threshold of the high efficiency (HE) cells to that of the standard (SE) cells in terms of their relative base-line diffusion lengths.

$$\frac{N_{ox}(HE)}{N_{ox}(S)} = \left(\frac{L_{no}(SE)}{L_{no}(HE)}\right)^2 \qquad (3)$$

The diffusion length in base-line standard cells is $\sim$ 170μm, corresponding to an efficiency of 14.5%. In a 16% efficient cell we have measured a diffusion length of $\sim$ 585μm. These data imply that the impurity thresholds in these high efficiency structures will be reduced by a factor of about 12.

Similarly a low efficiency (LE) cells will have a higher theshold. Experimental cells having a baseline efficiency of 10.6% and diffusion lengths $\sim$ 62μm were measured with 3×10^{13} cm^{3} Ti added. The resulting devices were 8.7% efficient and had diffusion lengths of 40μm. Thus the calculated threshold for Ti in these devices is 2.4 times longer than the value for our standard devices. The N_{ox}(Ti) for standard devices is $\sim 2.7\times10^{12}$ and in the LE devices the observed value equals $\sim 8\times10^{12}$, in good agreement with the calculated value of 6.5×10^{12}.

Experiments are in progress using both wide base and backfield structures; however, no data are available as yet.

There are two additional important impurity-related considerations which have not yet been adequately dealt with in the device analysis and impurity effect modeling. The first concerns non-uniform impurity distributions in the direction normal to the junction plane, which has been shown by deep level measurements to be present in virtually all completed solar cells. These non-uniform distributions are a consequence of intentional gettering processes or gettering which occurs during various process heat-treatment steps, including the junction formation step. In addition they may result from unintentional in-diffusion of contaminants during these same heat treatments. In the modeling analysis the effect of these profiles is included implicitly but only terms of the average impurity content. A more accurate description of the influence of the impurities requires considering where they are as well as how much. The analysis of these profile effects demands a more sophisticated model.

The second neglected consideration arises when one attempts to design a device which is maximally efficient, using silicon with a limited diffusion length. A backfield device with a limited base diffusion length will yield a maximum efficiency for base widths which are small with respect to the diffusion length. This can be shown with a simple device model; however, for a device structure with nonuniform diffusion lengths, the optimum thickness can be determined only with a distributed numerical model.

For this purpose we are presently implementing a computer model capable of analyzing these situations as-well-as providing the necessary functional relationships between the impurity concentrations and cell performance for backfield cells.

4. CONCLUSIONS

Nine new silicon ingots were grown during this quarter. A slight reduction in impurity concentration of V, Mo, and Cr in polycrystalline ingots has apparently eliminated the metal-rich inclusions formed in the first ingots of this type grown earlier in the program. Constitutional supercooling induced structural breakdown was confirmed as the source of the inclusions.

Very little lead can be incorporated into silicon ingots because of high vapor pressure of this element at the growth temperature. Thus Pb falls in a category with Zn, Na, and Mg as elements which make crystal growth difficult rather than degrading solar cell properties.

Measurement of deep level traps and cell efficiency for cells containing Mo, Ti, V, and Cr have corroborated previous conclusions regarding the fractions of atoms which are electrically active and their effects upon solar cell efficiency. No deep levels ascribable to Cu could be detected. This is consistent with solar cell I-V data and previous bulk lifetime measurements.

DLTS measurements made on polycrystalline materials show no appreciable segregation of Ti and V to structural defects when the metal concentrations are in the mid 10^{13} cm^{-3} range.

Experiments designated to determine the permanence of the effects of additional impurities and of impurities in cells under electrical bias are under way. The gettering of selected impurities by $POC\ell_3$ diffusion, $HC\ell$ oxidation, ion implanted junctions, and ion implant damage is being evaluated.

Preliminary modeling studies show that the effects of impurities in high efficiency cells will be quantitatively different from the effects in standard and low efficiency cells. Extension of the model to

non-uniform impurity distributions and to optimizing the cell base width for a spatially varying diffusion lengths is in progress.

5. PROGRAM STATUS

The program is on schedule with respect to assumed milestones.

5.1 Present Status

During the latest reporting period

- Nine new ingots, both crystalline and polycrystalline, were grown and characterized.
- Deep level trap concentrations were measured in single crystal ingots containing V, Mo, Cr, Ti, and Cu.
- It was shown that Ti and V do not segregate appreciably at grain boundaries in polycrystalline material at impurity concentrations of $\sim 10^{13}$ cm^{-3}.
- Experiments to determine the permanence of effects from additional impurities were initiated.
- Experiments to measure gettering of impurities in poly by $POC\ell_3$ and $HC\ell$ were initiated.
- Experiments to determine the interaction between impurities and ion implanted junctions and ion implant damage gettering were initiated.

5.2 Future Activity

During the next quarter, studies of impurity effects in polycrystalline cells will continue. Studies of gettering in polycrystalline material by $POC\ell_3$ and $HC\ell$ and of ion implant damage gettering in single crystal material will continue. Long term effects of electrical bias on cells containing selected impurities will be measured.

6. REFERENCES

1. R. H. Hopkins, et al., 11th Quarterly Report and Summary, Silicon Materials Task (Part 2) DOE/JPL 954331-78/3, July 1978.

2. R. H. Hopkins, et al., 5th Quarterly Report and Summary, Silicon Materials Task (Part 2) DOE/JPL 954331-77/1, January, 1977.

3. R. H. Hopkins, et al., 17th Quarterly Report and Summary Volume 1., Silicon Materials Task (Part 2) DOE/JPL 954331-80/9, January 1980.

4. R. H. Hopkins, et al. 18th Quarterly Report, Silicon Materials Task, April, 1980.

7. ACKNOWLEDGEMENTS

We would like to thank the following individuals whose contributions have been important to the success of this program: D. N. Schmidt (cell processing and testing), B. F. Westwood (process experiments and photolithography, A. M. Stewart (material characterization and web growth), H. F. Abt (metallization), C. F. Seiler (device measurements), S. Karako (DLTS measurements), T. Zigarovich (mask preparation), R. R. Adams and J. M. Bronnier (processing), D. Labor (manuscript preparation), and S. Farukhi (manuscript editing).